INTERNATIONAL JOURNAL OF
NUMERICAL ANALYSIS AND MODELING
Volume 23, Number 1, Pages 1–23

© 2026 Institute for Scientific
Computing and Information
doi: 10.4208/ijnam2026-1001

INTEGRATING PERIDYNAMIC THEORY WITH GROUND FISSURE MECHANICS: APPLICATION TO SONGZHUANG GROUND FISSURE STUDY

LINGFEI WANG, CHE WANG*, HUILI GONG, XIAOJUAN LI, HAIPENG GUO, XISHENG ZANG

Abstract. This study explores the application of Peridynamic (PD) theory in ground fissure modeling and simulation, focusing on the Songzhuang region in Beijing. Traditional methods often encounter difficulties in accurately capturing fissure formation and propagation due to discontinuities at the tips of the crack. The PD model, formulated through integral equations, effectively addresses these issues. It ensures model continuity and considers interactions within a non-local neighborhood of points. First, the study validates the numerical algorithm of the PD model through a two-dimensional tensile test of a plate with a central crack and a simulation of hidden ground fissures in Xi'an. The PD model is then applied to the Songzhuang area. The study integrated field drilling data to simulate fissure development. The results show fissures that grow in the expected direction, with significant subsidence and shear deformation on both sides. These findings provide new information on the impacts of ground fissures. Despite challenges such as high computational demands and the need for further model refinement, the study confirms the broad applicability of PD theory to geohazard mitigation. It also demonstrates the potential of the theory in improving urban planning and improving disaster response strategies.

Key words. Peridynamics, numerical simulation, ground fissure, fissure propagation, land subsidence.

1. Introduction

Peridynamic (PD) theory, developed to address the limitations of classical continuum mechanics, offers a robust framework for modeling discontinuities such as cracks and fissures. By utilizing integral equations, PD theory inherently manages crack formation and propagation, making it particularly suitable for simulating complex hazards like ground fissures.

Ground fissures are critical hazards that have been extensively studied in geosciences and geophysics. Their formation is the result of factors such as tectonic movements, changes in groundwater level, and human activities, including construction and mining. These interactions cause soil consolidation and localized subsidence[6, 13, 29], especially in urban areas with excessive groundwater extraction. In regions like Beijing, these processes have led to numerous subsidence funnels and over-extraction zones[3]. The Songzhuang area in the Tongzhou district is particularly affected, showing rapid fissure development and significant structural damage.

Early studies relied on field investigations and empirical models to characterize ground fissures and establish fissure strength criteria [5, 15, 19, 21, 23, 32, 37, 38]. However, these methods lacked the precision needed to understand the complex mechanisms of fissure formation and propagation. Research has shown that traditional numerical methods, such as finite element and finite difference methods, struggle with modeling discontinuities at crack tips and face significant challenges in

Received by the editors on January 2, 2025 and, accepted on June 3, 2025.
2000 *Mathematics Subject Classification.* 74S30, 86A60, 74A45.
*Corresponding author.

modeling ground fissure dynamics[1, 2, 4, 9, 10, 18, 27].These methods rely on local differential equations, which become inadequate near discontinuities where stress and strain fields exhibit singular behavior. Consequently, these approaches struggle to accurately capture fissure formation and propagation, leading to imprecise predictions.Therefore, a more advanced approach is required to accurately simulate fissure dynamics and improve geohazard prediction and mitigation strategies.

Empirical models also fail to describe the complex mechanisms of fissure dynamics. They often oversimplify interactions between geological layers and the dynamic processes driving fissure growth. To address these limitations, a more advanced approach is needed. PD theory, with its non-local integral formulation, offers a robust framework for accurately modeling crack initiation and growth. In the field of geology, the PD theory has demonstrated its applicability in simulating geological hazards such as landslides and rock fractures [22, 30]. These applications, displaying the versatility of PD in capturing the complex behavior of geological materials under stress, are crucial for understanding and predicting the occurrence of geological disasters.

Despite its potential, PD theory's application in ground fissure research remains under-explored. This study aims to fill this gap by integrating PD theory with empirical data to provide a detailed understanding of fissure propagation and evolution. The study employs PD theory to model ground fissures in the Songzhuang region of Beijing. PD theory, using integral equations, effectively handles discontinuities and simulates crack formation and propagation[16]. The non-local nature of PD theory considers interactions within a finite neighborhood of points, offering a more accurate representation of fissure dynamics compared to traditional methods.

The PD model is validated through two numerical experiments. First, a two-dimensional tensile test on a plate with a central crack demonstrates the model's accuracy in capturing crack propagation. Second, the simulation of hidden ground fissures in Xi'an replicates large-scale physical experiments, further confirming the model's reliability. The validated PD model is then applied to the Songzhuang area, integrating detailed field drilling data to simulate fissure development. This approach ensures the model accurately captures the morphology and dynamic changes of the fissures.

The primary objective of this study is to apply PD theory to model and simulate ground fissures in the Songzhuang region of Beijing. This study introduces PD theory as a robust framework for ground fissure dynamics, validated through numerical experiments and applied to real-world data. Key contributions include the integration of PD theory with empirical data, demonstrating its accuracy and feasibility, and providing new insights into fissure propagation and evolution. This research enhances our understanding of geohazard, offering practical solutions for urban planning and disaster mitigation.

The article is structured as follows: The introduction outlines the background and motivation for studying ground fissures using PD theory. Next, the literature review discusses traditional numerical methods and highlights the limitations that PD theory aims to address. The methodology section details the PD model formulation and its validation through numerical experiments. Subsequently, the results section presents the application of the PD model to the Songzhuang region, integrating field data to simulate fissure development. Finally, the discussion and conclusion emphasize the broader implications of the findings for geohazard mitigation, urban planning, and future research directions.

2. Peridynamic Model for Ground Fissure

This study employs a PD model based on integral equations to address the propagation of ground fissure. The integral equations in PD theory do not require the object to be continuous at every point, which gives it a natural advantage in handling discontinuities such as cracks and fractures. It effectively mitigating the impact of discontinuity-related issues [4, 33, 35, 36]. Furthermore, the non-local concept within PD theory closely emulates the expansion behavior of ground fissure[39]. This approach accounts for the interactions between a material point and all points within its neighborhood during dynamic calculations. And its results in a simulation of crack expansion that better adheres to the laws of physics.

2.1. Equation of Motion. PD theory, pioneered by Silling in 2000[24], offers a non-local perspective on material mechanics[11]. It solves spatial integral equations to describe material behavior. This theory aims to overcome the shortcomings of traditional continuum mechanics, particularly in handling discontinuities like fractures and crack propagation.

In classical mechanics, the principle of locality is a cornerstone, positing that material points interact only with their immediate neighbors. This limits its applicability to complex or extensive interaction scenarios. PD theory, however, is distinguished by its non-locality, where a material point's state is influenced by a broader neighborhood, reflecting a collective effect beyond immediate proximity. In PD's non-local model, a material point's condition is subject to a comprehensive influence from a defined range of other points.

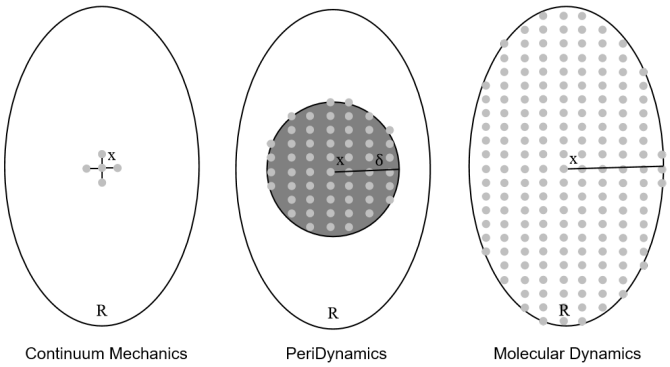

FIGURE 1. Schematic of a non-local model.

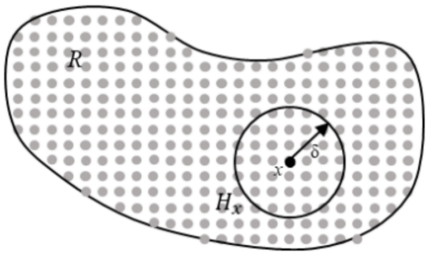

FIGURE 2. Peridynamic model for near-field dynamics.

As shown in Fig. 1 and Fig. 2, PD theory discretizes matter into material points with mass and volume, each bounded by a horizon. Within this horizon, interactions are calculated through integrals, determining mutual forces. The control equation of PD can be represented as:

$$\rho\ddot{u}(\mathbf{x},t) = \int_{H_x} f(u(\mathbf{x}',t) - u(\mathbf{x},t), \mathbf{x}' - \mathbf{x}) + b(\mathbf{x},t). \tag{1}$$

In Equation (1), ρ represents the material density, u represents the displacement of the material point, b represents the volume force acting on the material, δ denotes the near-field range centered on the material point with a neighborhood radius defined, and denotes the "force density" between the material point and other mass points within the near-field range.

After more than 20 years of development, the theory of PD has mainly been divided into two major categories: bond-based and state-based [7]. The bond-based model focuses on describing interactions by simulating the 'bonds' between material points, while the state-based model defines interactions directly based on the state of the material points. The state-based model is further divided into conventional and unconventional types to accommodate different types of material behavior.

To simplify the description and facilitate understanding, this article will focus on the bond-based peridynamic model. The relative position vector between the material points $\mathbf{x}$ and $\mathbf{x}'$ before the deformation of the object is defined as ξ, and the relative displacement vector between the two material points during the deformation process is defined as η, expressed as:

$$\xi = x' - x, \tag{2}$$

$$\eta = \mathbf{u}(x',t) - \mathbf{u}(x,t). \tag{3}$$

As shown in Fig. 3:

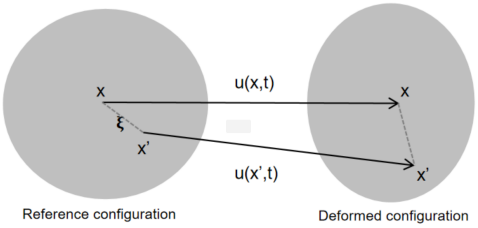

FIGURE 3. Schematic diagram of key deformation before and after.

In bond-based peridynamic, material points are interconnected through 'bonds' that behave like springs. These 'bonds' allow material points to interact with other material points within a certain range, simulating the force transmission process within the material. In Equation (1), the pairwise interaction function (ξ)represents the interaction force between material points, which corresponds to the constitutive relationship in classical continuum mechanics and is used to describe the mechanical response of the material. It is expressed as:

$$f = \begin{cases} ce^{\left(\frac{\xi+\eta}{|\xi+\eta|}\right)}, & |x'-x| \le \delta \\ 0, & \text{other} \end{cases}. \tag{4}$$

In this context, c represents the bond constant in peridynamic, and e denotes the elongation of the bond, which is expressed as:

$$e = |\xi + \eta| - |\xi|. \tag{5}$$

The bond constant c is determined via the principle of strain energy equivalence. This principle links the strain energy density from classical continuum mechanics to that in bond-based peridynamic. It ensures consistency in the material's mechanical behavior across both theories by equating the strain energy densities under similar deformation conditions.

$$C = \begin{cases} \frac{12E}{\pi\delta^4}, & \text{3D Problem} \\ \frac{63E}{4\pi\delta^4}, & \text{Plane Stress} \\ \frac{84E}{5\pi\delta^4}, & \text{Plane Strain} \end{cases}. \tag{6}$$

In this, E denotes the elastic modulus, and δ signifies the near-field range.

2.2. Failure Criteria. In PD, the instantaneous stretch ratio s of the bond is characterized by the relative deformation between the reference configuration and the current configuration, using the bond fracture criterion as the basis for determining damage, expressed as:

$$s = \frac{|\xi + \eta| - |\xi|}{|\xi|}. \tag{7}$$

When the stretch ratio of a bond exceeds its critical value s_0,6 the bond undergoes rupture, leading to damage in the local area of the material. This rupture irreversibly and permanently eliminates the interactive force between two material points, thereby affecting the overall load-bearing capacity of the material. The rupture of the bond can be formalized as:

$$\mu(t, \xi) = \begin{cases} 1, & s \le s_0 \\ 0, & s > s_0 \end{cases}. \tag{8}$$

In this, $\mu(t, \xi)$ represents the state function of bond, which ranges from 0 to 1. A value of 0 signifies an intact bond, while 1 indicates complete bond failure.

When a pair of interactive forces between material points is disrupted due to bond breakage, the mechanical connection between these two material points is eliminated, leading to a loss of local integrity in the material structure. However, when a material point undergoes deformation, it still maintains connections with other material points within its near-field range. Therefore, the failure of a single bond does not directly signify the material's overall fracture. To comprehensively assess the damage state of the material, a damage function is introduced to quantify the impact of local damage on the overall performance of the material. A damage function $\psi(x, t)$ is defined to describe the degree of damage of a material point, represented as Fig. 4:

$$\psi(x, t) = 1 - \int_{H_x} w \, dV_{x'} \Big/ \int_{H_x} dV_{x'}. \tag{9}$$

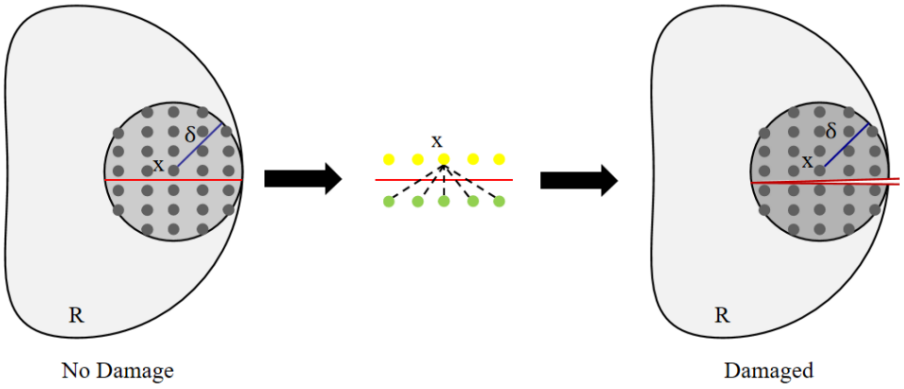

FIGURE 4. Schematic diagram of fracture.

2.3. Model Discretization. Model discretization involves breaking down the continuous medium into a finite set of material points[8, 12, 17]. Each point represents a tiny material element, encapsulating physical properties like mass and displacement.

The discretization process begins with the division of the spatial domain, where each material point interacts with other material points within its horizon. This interaction is described by a non-local integral equation, which can be transformed into a summation form during the discretization process. The equation (1) is then translated into a discrete summation form as:

$$\rho \ddot{u}_i^n = \sum_p f(u_p^n - u_i^n, x_p - x_i) V_p + b_i^n. \tag{10}$$

In Equation (10), u denotes the time step, while i and p represent a material point and another point within its neighborhood, respectively. Each material point i has a peridynamic domain within which integration is performed.

Typically, the peridynamic domain is chosen to be circular, which introduces certain geometric discrepancies during discretization. Since the discretized space is constructed from cubic elements, this leads to a misalignment between the boundaries of the cubes and the sphere at the edges. To address this issue, corrections are required.

As shown in Fig. 5, when the distance $\xi = |x_p - x_i|$ between the computational point x_p and the neighboring point is less than the peridynamic radius δ minus half the edge length of the discretization unit,that is $\xi > \delta - \frac{\Delta x}{2}$.No need for correction.however, when the distance is between $\delta - \frac{\Delta x}{2}$ and δ,that is $\delta - \frac{\Delta x}{2} < \xi < \delta$,A correction factor needs to be introduced to linearly adjust the values, expressed as: $V_{p(i)}$[25, 26]:

$$V_{p(i)} = \left(1 - \frac{\xi - (\delta - \frac{\Delta x}{2})}{\frac{\Delta x}{2}}\right). \tag{11}$$

The correction ensures a smooth transition of the model at the boundary.Points that are beyond the peridynamic domain are not calculated.

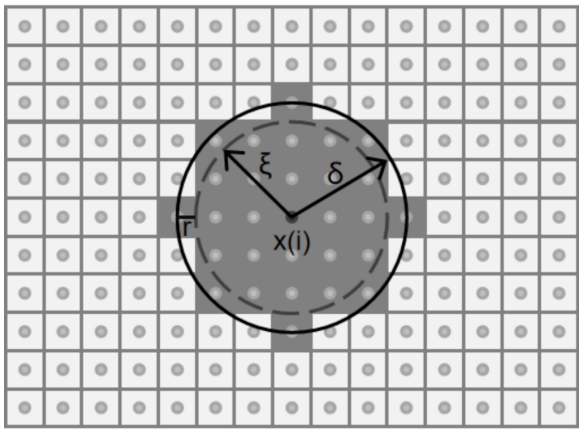

FIGURE 5. Schematic diagram of differences.

For temporal integration, the explicit Euler method is used for the neighboring points. At each time step Δt, the velocity and displacement of the material point are updated through Equation (12,13):

$$\dot{u}_i^{n+1} = \ddot{u}_i^n \Delta t + \dot{u}_i^n, \tag{12}$$

$$u_i^{n+1} = u_i^n \Delta t + u_i^n. \tag{13}$$

In Equation (13),u_i^n and $\dot{u}_i^n$ represent the velocity and acceleration of material point at time step n, respectively. By employing an explicit forward difference method, the velocity and displacement for the next time step can be determined, allowing for the precise tracking and updating of the motion state of each particle within continuous time steps.

3. Numerical Experiments of the Peridynamic Model

This chapter is dedicated to verifying the usability and precision of the enhanced PD model in the study of ground fissures. It commences with a two-dimensional tensile test on a plate featuring a central crack, thereby evaluating the model's capacity to simulate the progression of cracks. Subsequently, the chapter delves into the simulation of concealed ground fissures in Xi'an, under the scrutiny of complex geological conditions, to further test the model's robustness. These experimental assessments are vital for gauging the model's efficacy in capturing the dynamics of fissures. The chapter culminates in an analysis of the numerical outcomes, substantiating the model's reliability and its potential for practical application in real-world geohazard scenarios.

3.1. Introduction to Computational Programs. The PD program's was initially developed by Silling's team, utilizing the FORTRAN 90 language. This marked the first numerical computation application of the peridynamic method. As research progresses and technology evolves, the PD method's application scope has broadened. Various programming languages have been integrated, enhancing the field's toolkit.

Although PD is inherently a meshfree method,several commercial finite element software platforms (e.g., Abaqus PD Module, LS-DYNA) have introduced dedicated PD computational packages.Such integration has facilitated PD computation for researchers, lowering the barrier to PD method research in material and fracture mechanics and fostering rapid advancement in the field. In this study, MATLAB was chosen for developing the computational program due to its flexibility in implementing meshfree algorithms.The algorithm flowchart is shown in Fig. 6.

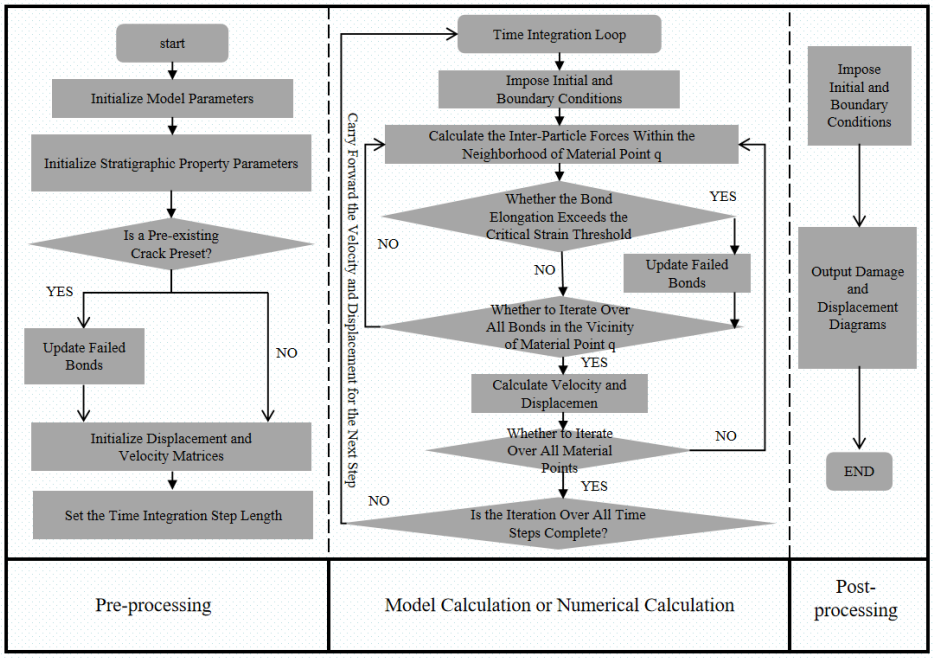

FIGURE 6. Algorithm flowchart.

3.2. Numerical Models. To verify the feasibility of the aforementioned numerical computation model, this study has designed two numerical model experiments for validation. The first is a two-dimensional plate tensile test with a pre-existing central crack. The second is a simulation based on the physical experiment of fault rupture propagation in Xi'an.

3.2.1. Tensile of a Cracked Two-Dimensional Plate. This section's experiment conducts a numerical simulation of a two-dimensional plate with a central crack. The model dimensions are shown in Fig. 7, with a length of 0.05 meters and a width of 0.05 meters. There is a pre-existing horizontal crack at the center of the model, with a length of 0.01 meters. The material properties are set with a Young's modulus $E = 192GPa$, a Poisson's ratio $\mathbf{v} = 1/3$, and a mass density of 8000 kg/m^3.

In this experiment, different loads will be applied to the model, with the upper and lower boundaries having a prescribed displacement velocity of 20 m/s. The damage results at steps 750, 1000, and 1250 are shown in Fig. 8.

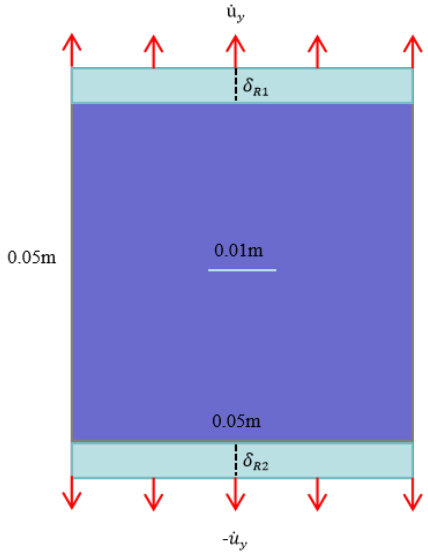

FIGURE 7. Schematic diagram of a cracked 2D plate model.

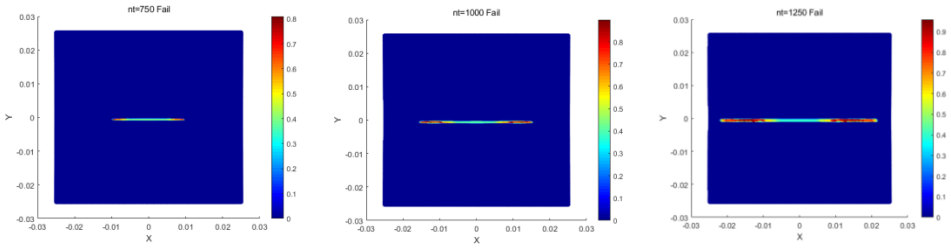

FIGURE 8. 8 (a) Damage diagram at step 750 (b) Damage diagram at step 1000 (c) Damage diagram at step 1250.

The upper and lower boundaries are set with a prescribed displacement velocity of 50 m/s, and the damage results at steps 750, 1000, and 1250 are illustrated in Fig. 9.

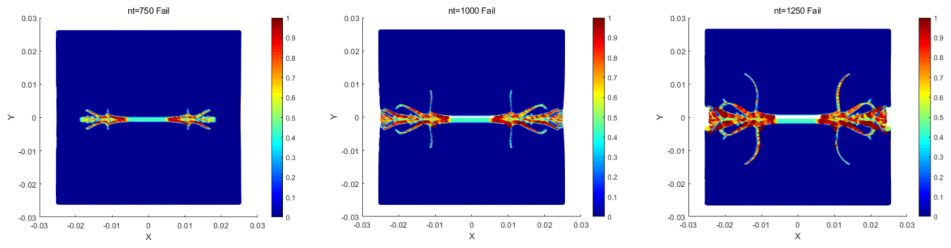

FIGURE 9. (a) Damage diagram at step 750 (b) Damage diagram at step 1000 (c) Damage diagram at step 1250.

From the Fig. 9, it can be observed that different boundary conditions result in different crack propagation patterns. The faster the stretching velocity,

the quicker the crack propagates. At a velocity of 20 m/s, the ground fissure remains unbranched. In contrast, at 50 m/s, clear branching of the ground fissure is observable. This model demonstrates the advantage of the peridynamic model in autonomously generating cracks, capable of simulating more complex crack branching phenomena.

While methods based on the PD model demonstrate significant advantages in handling discontinuities at crack tips, inevitable errors are introduced during simulations. These errors primarily originate from the discretization process?, where continuous media must be discretized into material point grids for PD computations. The discretization parameters critically influence both computational accuracy and efficiency.This study evaluates model discretization rationality by comparing results under different grid resolutions. Taking a cracked 2D plate tensile experiment under 20 m/s loading as an example, for a 0.5 m 0.5 m model, we test discretization point configurations of 100100, 200200, 300300, 400400, and 500500 in the x-y directions. This systematic resolution comparison aims to validate both the accuracy of crack propagation length predictions and solution convergence under varying grid densities. From Fig. 10, it can be observed that as the mesh

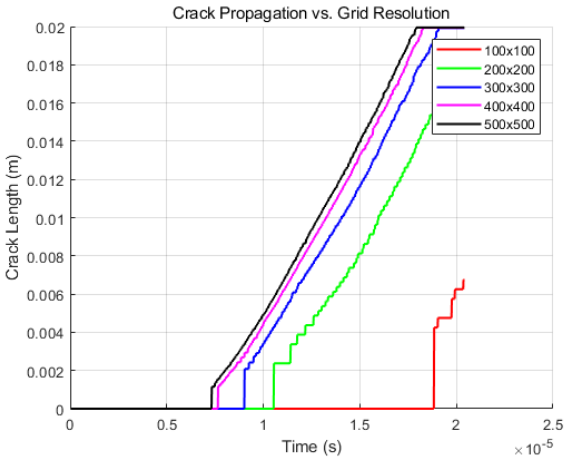

FIGURE 10. Simulation results of crack length propagation under different mesh resolutions at the same time step.

resolution increases, the simulated crack length gradually stabilizes and converges under a fixed total time step. At lower mesh resolutions (e.g., 100100 and 200200), the crack length propagation curve remains relatively flat in the initial stage and then rises rapidly at a certain time point, indicating the onset of accelerated crack propagation. With increasing mesh resolution (300300, 400400, 500500), the initiation point and propagation rate of crack growth become more consistent, and the curves appear smoother. This demonstrates that higher-resolution meshes can more accurately capture crack propagation behavior and reduce the impact of discretization errors. Additionally, significant differences in crack lengths are observed across resolutions at most time points, particularly during the rapid propagation phase, where predictions from low-resolution meshes deviate substantially from those of high-resolution meshes. This suggests that excessively low resolutions in peridynamic simulations may lead to inaccuracies and larger errors. However, due to the non-local integral nature of peridynamic, excessive discrete points (e.g., 500500

generating 250,000 material points, each requiring local integral calculations within its peridynamic horizon) drastically reduce computational efficiency. Therefore, selecting an appropriate mesh resolution is critical for accurately predicting crack propagation while balancing computational costs.

3.2.2. Numerical Simulation of the Large-Scale Physical Experiment of Fault Rupture Propagation. This section of the experiment correlates with the physical fault rupture propagation experiment in Xi'an, utilizing a sand-box model to emulate the movement of a concealed fault. The box dimensions are 5.0 meters in length, 1.5 meters in width, and 3.0 meters in height. The sides are enclosed with acrylic glass, the top plate's bottom is adjustable and controlled by a set of jacks to simulate subsidence, and the bottom plate is stationary. Acrylic glass is positioned at a 30 angle within the soil to mimic the hidden fault. The soil mass consists of compacted, remolded loess soil.

For this study, a segment of the physical experiment is selected for numerical simulation, creating a two-dimensional model as depicted in Fig. 11, which is then discretized for analysis.

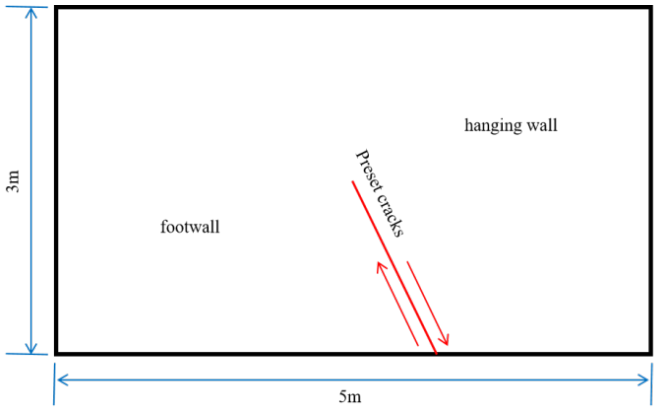

FIGURE 11. Schematic diagram of a hidden ground crack propagation in a 2D cross-sectional model.

The material is set with an elastic modulus of $\mathbf{E} = 8.5MPa$, a Poisson's ratio v =0.3 and a mass density of 1700 kg/m3. The discretization parameters are set with 206 material points in the x-direction (including the virtual boundaries on both sides), 123 material points in the y-direction (including the virtual boundary at the bottom of the model), with a material point spacing of Δ =0.025, a near-field range of=3.015Δ, and a critical stretch ratio based on experiments related to the tensile behavior of geomaterials[31, 28]. It is found that most clay-like porous media will fracture when the stretch ratio exceeds 0.003, thus a critical stretch ratio of 0.003 is adopted.

Fig. 12 and Fig. 13 illustrate the results of the subsurface fault rupture expansion at 250, 300, 350, 400, 450, and 500 time steps. It can be observed that reverse-dipping faults appear first from the bottom up as the step length increases. When these reverse-dipping faults develop to a certain extent, vertical faults from the ground surface downward emerge. This phenomenon is essentially consistent with the development mode of ground faults in physical experiments[21].

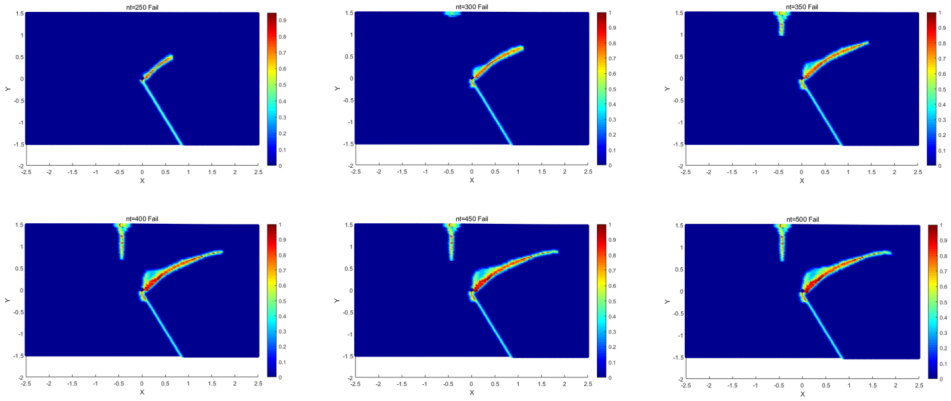

FIGURE 12. Displacement at different time steps($nt = 250, nt = 300, nt = 350, nt = 400, nt = 450, nt = 500$).

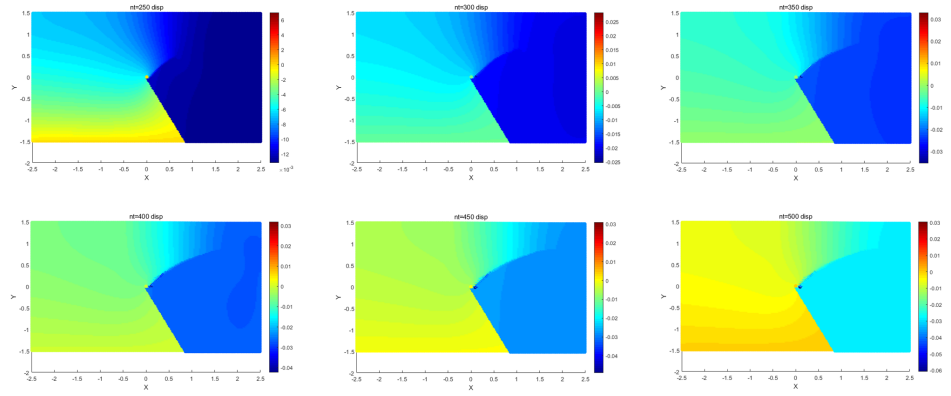

FIGURE 13. Damage at different time steps($nt = 250, nt = 300, nt = 350, nt = 400, nt = 450, nt = 500$).

4. Application of the Songzhuang Ground Crack Model

This chapter applies the validated PD model to simulate ground fissures in the Songzhuang region. It begins by integrating field drilling data to construct an accurate geological model of the area. The chapter then details the application of the PD model to simulate the development and evolution of ground fissures under local geological conditions. The results are compared with observed fissure patterns to assess the model's predictive capability. The chapter concludes by discussing the practical implications of the simulation for urban planning and geohazard mitigation in the Songzhuang region, demonstrating the model's utility in real-world applications.

4.1. Overview of Songzhuang Ground Cracks. In recent years, the development and construction of the urban deputy center in Tongzhou District, Beijing, have coincided with the swift emergence of ground fissures in Songzhuang Town. This has led to issues like cracks appearing in residential buildings, walls, and roads. Despite the severity of these issues, there is a notable lack of research on the rupture and expansion mechanisms of the Songzhuang ground fissures. This gap

in knowledge exacerbates the impact and losses attributed to the ground fissure problem.

4.1.1. Geological Environment. Tongzhou District's Songzhuang Town, situated on the northeastern outskirts of Beijing,boasts a terrain shaped by the alluvial plains of the Yongding and Wenyu Rivers, sloping from northwest to southeast. The climate is a warm temperate semi-humid and semi-arid continental monsoon climate, marked by significant temperature variations and clear seasonal shifts. The geomorphology is dominated by alluvial plains, including river terraces and floodplains. Geologically, the area features Quaternary loose sedimentary strata, interspersed with sands and clays, indicative of the rivers' extensive sedimentary activities. The underlying bedrock is uneven, and the sedimentary strata's thickness decreases from east to west[20, 34].As shown in Fig. 14.

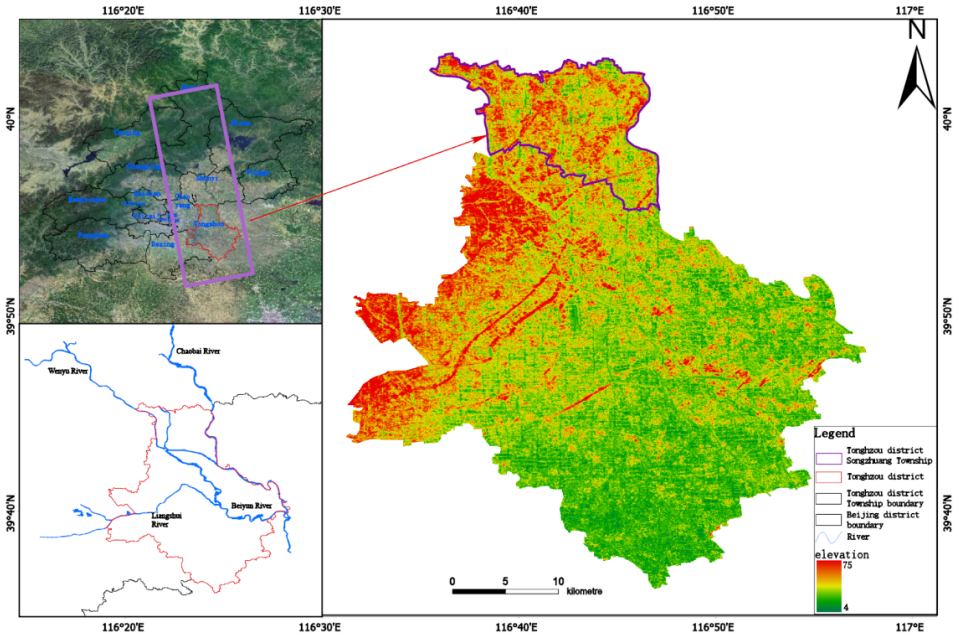

FIGURE 14. Songzhuang town, Tongzhou district, Beijing city.

Tongzhou District, with rivers like the Chaobai, Wenyu, and the North Canal, is part of the Haihe River Basin. Its groundwater system is structured into four distinct aquifers. The shallow aquifer consists of fine to medium sands, and the deeper aquifers are predominantly coarse sand and gravel. Shallow groundwater is primarily replenished by precipitation, while deep groundwater sources depend on lateral flow and contributions from the shallower layers.

4.1.2. Overview of Ground Cracks. Since the end of the Mesozoic era, the Beijing plain area has undergone a series of tectonic evolutions, mainly in the NE and NW directions. Among these structures, the NE- and NNE-trending faults play a dominant role in the regional stability,As shown in Fig. 15.The Nanyuan-Tongxian fault is an important controlling fault within Tongzhou District and is considered the boundary line between the Beijing Depression and the Daxing Uplift. This fault significantly influences the distribution of the Cenozoic strata and other

geological formations in the Tongzhou area, with the northwest side having greater thicknesses of Quaternary and compressible layers compared to the southeast side.

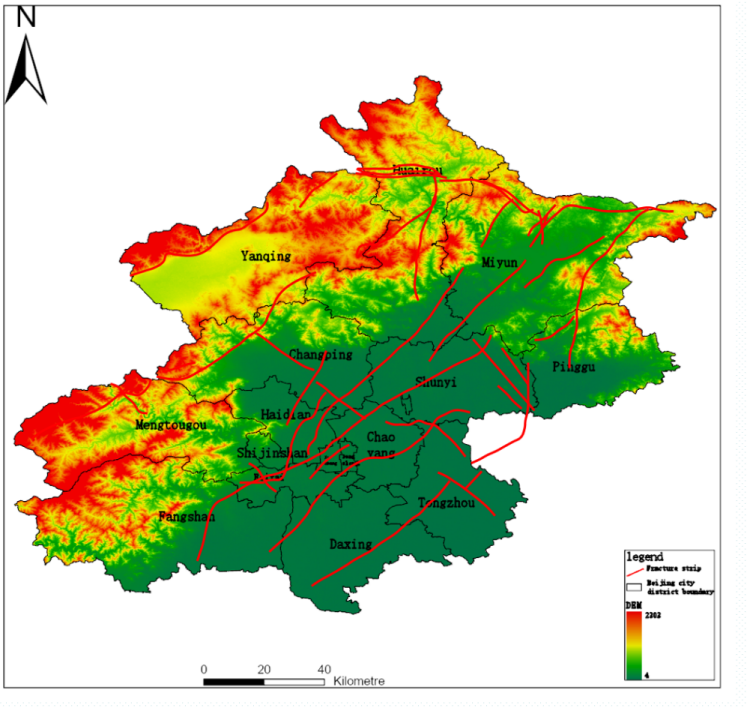

FIGURE 15. Fault zone in the Beijing area.

The Nanyuan-Tongxian fault begins in the southern part of Zhuozhou City, Hebei Province, and extends northeastward, traversing locations such as Diaowo, Chenjiafang, Nanyuan, and Tongzhou. It continues to the southeast of Shunyi District, near Beiwu and Nanzhuangtou, spanning roughly 110 km in total. The fault's general orientation is NE35 to 50, dipping northwest at an angle of 60 to 75. It is characterized as a high-angle normal fault, with the northwest block descending and the southeast block uplifting relatively.

As shown in Fig. 16 and Fig. 17. The Songzhuang ground fissure is a rapidly developing fissure discovered in recent years. Research has found that there is a significant spatial difference in the thickness of the depositable layers on both sides of the fault zone in the Songzhuang area, characterized by a much greater thickness on the northwest side compared to the southeast side.This difference may be related to the complexity and heterogeneity of the geological structures within the area. The relatively larger depositable layer thickness on the northwest side may be influenced by fault zone activity and tectonic deformation, resulting in the formation of thicker strata.

In 2017, Zhao Long and colleagues conducted a detailed investigation of the Songzhuang ground fissure in Beijing using groundwater monitoring, geophysical exploration, and drilling techniques, concluding that the development of the fissure is jointly influenced by geological structures and the thickness of sedimentary layers[37]. Tian Miaozhuang and colleagues used high-density electrical methods

FIGURE 16. Field photograph of Songzhuang ground cracks (Beijing geological environment institute).

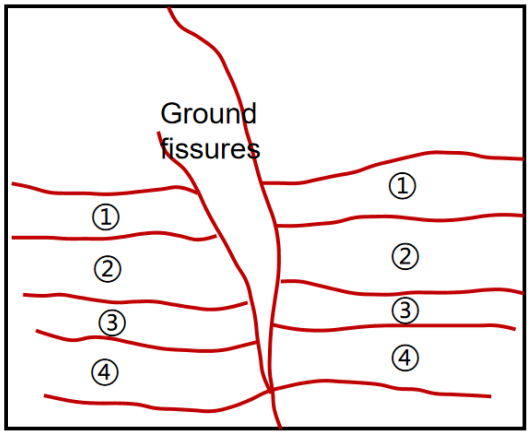

FIGURE 17. Schematic diagram of Songzhuang ground cracks.

for shallow exploration of the ground fissure and verified through inversion that it exhibits a tensile fracture pattern[28]. Liu Decheng employed the grey relational analysis method to assess the risk of ground fissure disasters in Tongzhou District[15]. Kong Xiangru and colleagues detected the Songzhuang ground fissure using PS-InSAR technology and concluded from their research that there are subsidence centers on each side of the fissure, with significant subsidence gradient changes in the direction perpendicular to the fissure zone, indicating pronounced

differential subsidence phenomena[14]. Meng Zhenjiang and colleagues numerically simulated the Songzhuang ground fissure using the finite difference method[20].

4.2. Numerical Simulation of Songzhuang Ground Cracks. This study focuses on Xu Xinzhuang and Shuangbu Tou Village, regions with prominent ground fissures. Before conducting numerical simulation of the ground fissures, the drilling data from this area were meticulously categorized and organized. Six sets of drilling data that could be paired relatively were selected as the basic data for this experiment. The positions of the six drilling wells are marked as A1, A2, A3, A4, A5 and A6, respectively. Based on the drilling locations, three cross-sections along the NW-SE direction, namely A1-A2, A3-A4, and A5-A6, were established for the numerical simulation of the ground fissures. The choice of this direction aims to align with the main development trend of the fissures to more accurately capture the morphology and dynamic changes of the cracks. As shown in Fig. 18:

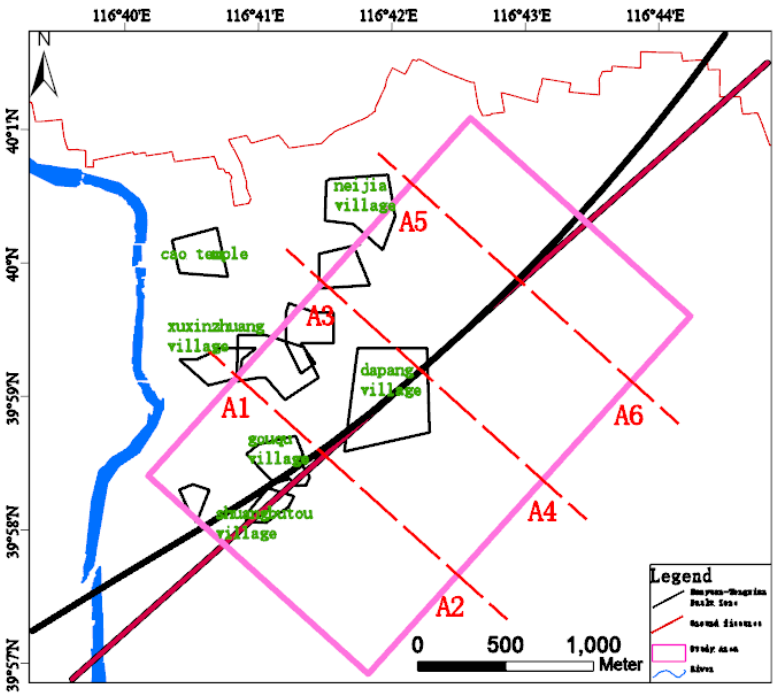

FIGURE 18. Cross-section selection diagram.

The Songzhuang ground fissure cross-sectional model constructed in this study has specific dimensions of 100 meters in length and 50 meters in height. In terms of stratigraphic setting, based on the refinement of drilling data, the strata are simplified and abstracted into six layers, from top to bottom, as the silty clay layer, Silty Clay Loam1 layer, silt1 layer, Silty Clay Loam2 layer, silt2 layer, and the bedrock layer. The specific division of stratigraphic heights can be seen in Table 1.

Based on the stratigraphic division of the A1-A2 cross-section, a numerical calculation model for the Songzhuang ground fissure A1-A2 cross-section was established, and virtual boundary layers were added to the boundaries for the application of loads, as shown in Fig. 19.

TABLE 1. Stratigraphic division of Songzhuang ground crack cross-section.

Cross- Section	Hanging Wall (m)	Foot Wall (m)
A1-A2	4 ,8 ,10 ,14 ,8 ,6	10 ,6 ,10 ,12 ,6 ,6
A3-A4	4 ,8 ,8 ,14 ,10 ,6	10 ,6 ,8 ,12 ,8 ,6
A5-A6	4 ,6 ,12 ,12 ,10 ,6	12 ,4 ,6 ,14 ,8 ,6

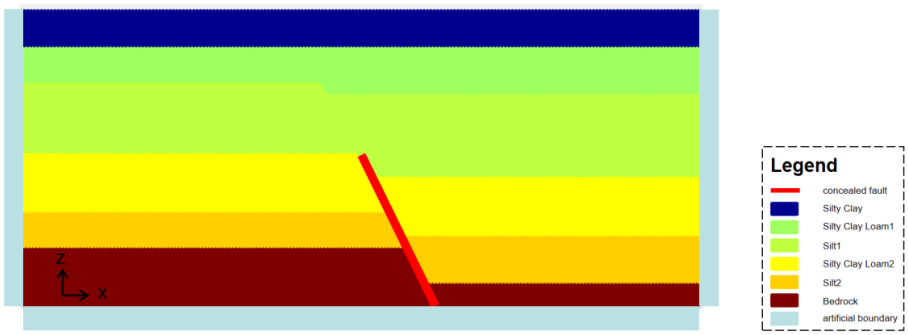

FIGURE 19. Numerical computational model for the Songzhuang ground crack section A1-A2.

The scale of the profile model used to simulate the Songzhuang ground fissure is specifically 100m in length and 50m in height. In the simulation, the A1-A2 profile is used as an example. The X direction is discretized into 200 material points, and the Y direction into 100 material points, with a spacing Δx of 0.5m between adjacent material points. At the same time, virtual boundary layers are set on both sides and at the bottom, with a length of Δx . The peridynamic domain size is set to as 3.015 Δx to ensure the non-local validity of the simulation, and the critical stretch is adopted as 0.003 to reflect the tensile properties of rock. Specific parameters are shown in Table 2 and Table 3.

TABLE 2. Stratigraphic parameters of the Songzhuang ground fissure profile A1-A2.

Serial Number	Stratum	Young's Modulus (Pa)	Poisson's Ratio	Mass Density (kg/m^3)
1	Silty Clay	4.0×10^6	0.30	1700
2	Silty Clay Loam1	8.5×10^6	0.35	1600
3	Silt1	9.0×10^6	0.30	1800
4	Silty Clay Loam2	1.05×10^7	0.30	1600
5	Silt2	1.2×10^7	0.30	1900
6	Bedrock	1.40×10^10	0.25	2500

TABLE 3. Peri-field dynamic parameters of Songzhuang ground fissure profile A1-A2.

Parameter Name	**Parameter Value**
Material Point Spacing Δ	0.0005 km
Volume of a Single Material Point ΔV	1.0×10^{-3} km^3
Total Number of Material Points in the X Direction	206
Total Number of Material Points in the Y Direction	103
Neighborhood Radius or Interaction Radius δ	3.015Δ
Critical Stretch Ratio or Critical Strain Ratio	1 (without considering damage) 0.003 (considering damage)

The boundary conditions incorporate both Dirichlet and Neumann types to precisely reflect the impact of the actual geological environment and external forces on crack propagation. The left and right boundaries of the model are fixed in the X-direction with displacement constrained to zero, simulating the lateral restriction of the surrounding strata on the study area. The bottom boundary is divided into two parts: 1) The left bottom boundary of the pre - set crack has fixed Y - direction displacement (Dirichlet boundary conditions), simulating the restriction of a rigid basement on vertical displacement. 2) The right bottom boundary of the pre-set crack is a free boundary, allowing vertical deformation to reflect ground - crack expansion due to fracturing of the basement. Also, the vertical effective stress converted from pore - water pressure is applied as body force (Neumann boundary conditions), reflecting the driving effect of pore - water - pressure changes from groundwater extraction.

4.3. Results Analysis. Considering the impact of time steps on the convergence of equation solutions, the A1-A2 profile was simulated for 330 time steps (not representing real time), and the damage of the ground fissure at time steps 100, 150, 200, 250, 300, and 330 is shown in Fig. 20.

From time steps 100 to 300, the ground fissure damage worsened. Between 100 and 150, damage emerged at the top of the reverse-dipping fissure, with localized stress concentration. At step 200, the damage area expanded, the fissure became more defined, and initial branching occurred, forming a slender reverse-dipping fissure opposite the pre-set one. By step 250, the fissure extended toward the right upper part. At step 300, the damage was severe, with a large, complex fissure area and an upright fissure developing downward from the top of the reverse-dipping fissure. At step 330, small fissures formed between the reverse-dipping and upright ones, creating a complex network, with the upright fissure continuing to grow downward.

The whole development can be divided into three stages: initiation,growth and expansion, as shown in Fig. 21. During the initial simulation phase, tensile stress concentration occurs at the tip of concealed ground fissures due to reactivation of basement faults, triggering reverse-dip fractures to propagate upward into the hanging wall at 455, forming the initial rupture zone.This phenomenon is closely related to the activity of basement fault zones and aligns with the regional tectonic

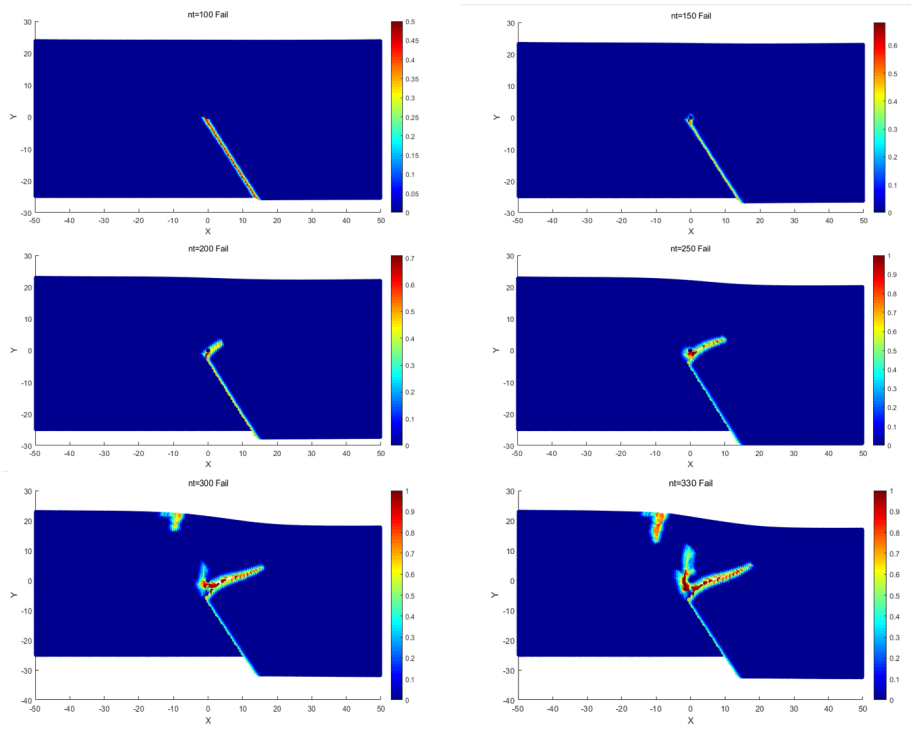

FIGURE 20. Damage maps of the A1-A2 profile at $100nt$, $150nt$, $200nt$, $250nt$, $300nt$, and $330nt$.

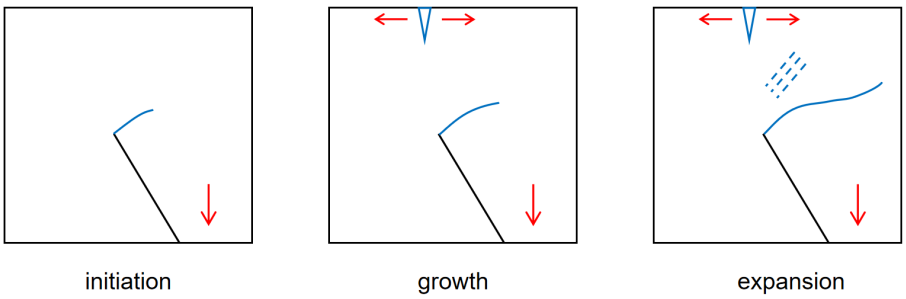

FIGURE 21. The development trend of ground fissures: initiation, growth, and expansion.

setting of transtensional movement along the Nanyuan-Tongxian Fault Zone.The preferential development of reverse-dip fractures indicates that stress release from basement faults dominates fissure initiation.

As simulation time progresses, when reverse-dip fractures extend to approximately 10 meters below the surface, differential settlement in overlying soil layers intensifies, leading to vertically downward surface cracks that intersect with reverse-dip fractures forming a “Y”-shaped junction.The damage field reveals significantly

increased settlement in the hanging wall and localized uplift at fracture intersections, indicating that groundwater over-exploitation-induced pore pressure decline causes compression in clay layers, exacerbating surface tensile rupture.

At the mature stage, the main rupture surface becomes fully interconnected.Secondary feather-like fractures with 0.8-1.2 m spacing develop on both sides of the reverse-dip fracture initiation points, strongly correlated with lithological heterogeneity. As shown in Table 2, the higher Young's modulus of silty sand layers compared to silty clay layers leads to stress concentration more easily in clay layers, inducing secondary fracture formation.

During crack propagation, the damage zone gradually expands, particularly near the crack tip where damage intensity is most pronounced.In early stages, damage concentrates around the crack tip, then progressively extends outward with crack advancement, ultimately forming extensive damaged areas. This process correlates with cumulative material damage caused by stress concentration during fracture propagation.

Subsequently, ground fissure propagation simulations were conducted on the A1-A2, A3-A4 and A5-A6 profiles for 350 time steps (not representing real time), with results shown in Fig. 22, Fig. 23, Fig. 24.

5. Conclusion and Outlook

5.1. Conclusion. This study delves into the methodologies for studying ground cracks, critically analyzing existing methods and their limitations in handling the nonlinear complexities and unpredictability inherent in such systems. Traditional approaches often falter when dealing with discontinuities at the tips of cracks and voids. To address this, the study introduces a novel approach based on PD theory, which adeptly handles these discontinuities. The paper concisely covers: (1) A comparison between traditional methods and the PD-based non-local model, capable of autonomously generating damage cracks. (2) Model verification through numerical experiments. Two numerical experiments, tensile of a cracked two-dimensional plate and numerical simulation of a large-scale physical experiment of fault rupture propagation, were conducted, and the results were highly consistent with the expected outcomes, confirming the correctness of the model. (3) Application of the model to Songzhuang ground cracks. Ground crack issues are geological disasters caused by multiple factors such as ground subsidence and tectonic fractures.In the application process, actual drilling data were utilized, combined with the results of geological exploration, to conduct a detailed simulation analysis of the ground cracks in the Songzhuang area, further verifying the practicality and accuracy of the model.(4) Geohazard Mitigation.This study has confirmed the application of PD theory in the mitigation of geological disasters. The PD model holds great potential in strengthening urban planning and improving disaster response strategies, offering practical references for managing geological disasters in areas susceptible to ground fissures.

5.2. Outlook. The PD method for ground crack analysis faces notable challenges: (1) High Computational Demand: The extensive particle/nodal simulations and non-local interactions in PD can lead to high computational loads, affecting efficiency in large-scale projects. (2) Incomplete Contact Models: PD's current contact models need enhancement for precise simulation of material interactions in complex engineering environments. (3) Diverse Material Properties: The variability of geological materials' properties requires adaptable PD models to suit different

scenarios. (4) Numerical Stability: PD's non-local interactions may trigger instability during simulations of material fragmentation and deformation, requiring ongoing optimization for stability.(5) Potential for Multi-Hazard Applications: For instance:In landslide studies, PD can simulate the failure processes of rock-soil masses and reveal the evolution mechanisms of sliding surfaces. For debris flow modeling, it captures solid-liquid phase coupling behaviors through non-local interactions to enhance the accuracy of flow path predictions. Regarding ground collapse, PD integrates the propagation of underground cavities to enable predictive early-warning for collapse genesis.

Further research and technical advancements are essential to refine algorithms and deepen the understanding of material behaviors and scenarios, with the aim of overcoming these challenges and expanding PD's application in ground crack studies.

Acknowledgments

This work was supported by the Open Fund of Hebei Cangzhou Groundwater and Land Subsidence National Observation and Research Station, China [No. CGL0S-2022-06]; National Natural Science Foundation of China, Key Program [No. 41930109]; National Natural Science Foundation of China, General Program [No. 42271487]; and R&D Program of Beijing Municipal Education Commission, China [No. KM202310028007].

References

[1] Bray, J.D., Seed, R.B., Cluff, L.S., Seed, H.B., 1994. Earthquake Fault Rupture Propagation Through Soil. J. Geotech. Eng. 120(3), 543-561.

[2] Chen, L.W., 2007. Study on the Mechanism of Ground Fissure Propagation. Ph.D. Dissertation, Chang'an University, China.

[3] Chen, B.B., Gong, H.L., Li, X.J., Lei, K.C., Du, Z.F., 2012. Evolution of the Groundwater System and the Process of Ground Subsidence in Beijing. J. Jilin Univ. (Earth Sci. Ed.) 42(S1), 373-379.

[4] Chen, F., Wang, Y.C., Jiang, W., Zheng, S.H., 2021. Numerical simulation of ground movement induced by water and sand gushing in subway through fault based on DEM-CFD. Computers and Geotechnics 139, 104282.

[5] Chen, Z.X., Liu, Y.H., Ni, W.K., Zhao, F.S., 1994. Zonation of Damage Strength and Determination of Safe Distance of Buildings At Geofracture Site in DATONG City. J. Geol. Hazards Control China 5(Supplement), 339-344.

[6] Dong, Y., Zhang, M.S., Liu, J., Zhang, X.S., Feng, L., 2019. Coupling Relationship between Groundwater and Ground Fissures of Land Subsidence in Xi'an City and Risk Prevention and Control Technology. Northwest Geol. 52(2), 95-102.

[7] Du, Q., Tian, L., Zhao, X., 2019. A convergent adaptive finite element algorithm for nonlocal diffusion and peridynamic models. SIAM J. Numer. Anal. 51(2), 1211-1234.

[8] Gao, Y.L., He, X.M., Lin, T., Lin, Y.P., 2023. Fully Decoupled Energy-Stable Numerical Schemes for Two-Phase Coupled Porous Media and Free Flow with Different Densities and Viscosities. ESAIM Math. Model. Numer. Anal. 57(3), 1323-1354.

[9] Guo, E.D., Shao, G.B., Bo, J.S., Shi, Z.J., 2002. A method for earthquake rupture analysis of overlying soil site. Earthq. Eng. Eng. Vib. 22(5), 122-126.

[10] Han, A.J., Ran, Y.K., Xu, X.W., 2002. Preliminary Study on the Width and Displacement of Future Surface Rupture Zones of Hidden Active Faults. Seismol. Geol. 24(4), 484-494.

[11] He, X.M., Zhao, X., Zuo, W.M., 2020. Maximum Principles for a Fully Nonlinear Nonlocal Equation on Unbounded Domains. Commun. Pure Appl. Anal. 19(9), 4387-4399.

[12] He, X.M., Meng, Y.X., Squassina, M., 2023. Multiplicity of Normalized Solutions for the Fractional Schrodinger-Poisson System with Doubly Critical Growth. Topol. Methods Nonlinear Anal. 1-26.

[13] Jiang, Y., Wang, R., Tian, F., Liu, M.K., 2014. Study on the Relationship between Ground Subsidence and Ground Fissures in Beijing Area. Urban Geol. 9(4), 6-10.

[14] Kong, X.R., Luo, Y., Liu, H., Wang, H.X., Zhao, L., Sha, T., 2021. Application of PS-InSAR Technology in Monitoring Ground Subsidence in Tongzhou District, Beijing. Urban Geol. 16(1), 25-31.
[15] Liu, D.C., He, J., 2008. Evaluation and Zoning of Ground Subsidence Hazard in Tongzhou District, Beijing. J. Geol. Hazards Control China (3), 158-159, 162.
[16] Liu, Y., 2023. A Study on the Genesis Mechanism and Prevention and Control Strategies of Bedrock Rupture-Type Ground Fissures in the Kenya Rift. Ph.D. Dissertation, Chang'an University, China.
[17] Lin, Y.P., Xiu, Y., Zhang, S.Y., 2022. A Mixed Finite Element Method on Polytopal Mesh. Commun. Appl. Math. Comput. 4(4), 1374-1385.
[18] Lin, Y.P., 2023. A Priori L2 Error Estimates for Galerkin Approximations to Semilinear Parabolic Integro-Differential Equations. Cybernetics, Robotics and Control, 421-434.
[19] Lu, Q.Z., Zhao, F.K., Peng, J.B., Bo, F., 2013. A Review of the Research on the Propagation and Expansion of Hidden Ground Fissures. J. Eng. Geol. 21(6), 898-907.
[20] Meng, Z.J., Peng, J.B., Li, C. et al., 2023. Simulation Study on the Activity Characteristics and Genesis Mechanism of Coupled-Type Ground Fissures: A Case Study of Songzhuang Ground Fissures in Beijing. J. Hydrogeol. Eng. Geol. 50(3), 138-148.
[21] Peng, J.B., Chen, L.W., Huang, Q.B. et al., 2008. A Large-scale Physical Simulation Test Study on the Propagation and Expansion of Ground Fissures. Chin. J. Geophys. 51(6), 1826-1834.
[22] Qin, M.Q., Yang, D.S., Jia, Y., Zhou, Y., 2024. Peridynamic modeling of hydraulic fracture interaction with natural fractures in fractured rock mass. Eng. Fract. Mech. 307, 110299.
[23] Shi, Y.L., Men, Y.M., Peng, J.B., Huang, Q.B., Liu, H.J., Chen, L.W., 2008. Numerical Simulation of Ground Fissures Propagation Expansion in Xi'an Urban Area. J. Hydrogeol. Eng. Geol. (6), 56-60.
[24] Silling, S.A., 2000. Reformulation of Elasticity Theory for Discontinuities and Long-Range Forces. J. Mech. Phys. Solids 48(1), 175-209.
[25] Silling, S.A., Askari, E., 2005. A meshfree method based on the peridynamic model of solid mechanics. Comput. Struct. 83(17-18), 1526-1535.
[26] Silling, S.A., Epton, M., Weckner, O., Xu, J., Askari, E., 2007. Peridynamic States and Constitutive Modeling. J. Elasticity 88, 151-184.
[27] Sun, P., 2007. Experimental Study on the Fracture Characteristics of Loess. Ph.D. Dissertation, Chang'an University, China.
[28] Tian, M.Z., Wang, R., Zhao, L. et al., 2017. Application of High-Density Electrical Method in Ground Fissures of Songzhuang, Beijing. Shanghai Land Resour. 38(3), 90-93.
[29] Wang, S., Zhang, L.Q., Zhou, J. et al., 2023. Land Subsidence Monitoring and Geo-Hazard Development Characteristics of Honghui Mining Area in Gansu Province Based on SBAS-InSAR Time Series Analysis. J. Eng. Geol. 31(6), 1951-1963.
[30] Wang, R.H., Li, S.F., Liu, Y. et al., 2024. Peridynamic-based large-deformation simulations for near-fault landslides considering soil uncertainty. Comput. Geotech. 168, 106128.
[31] Yan, L.F., 2013. Experimental Study on the Tensile Properties of Viscous Clay. M.Sc. Thesis, Nanjing University, China.
[32] Yang, Y.L., 2021. Experimental Study on the Propagation and Expansion Model of Synsedimentary Ground Fissures in Sand-Soil Interbeds. M.Sc. Thesis, Chang'an University, China.
[33] Yutaka, F., Taiki, S., 2023. 3-D coupled peridynamics and discrete element method for fracture and post-fracture behavior of soil-like materials. Computers and Geotechnics 158, 105372.
[34] Zhang, Y.Y., He, X., Du, H.W., 2021. Application of three-dimensional geological model to engineering construction layer in Tongzhou District of Beijing. Urban Geol. (03), 260-266.
[35] Zhang, S.Y., Nie, Y.F., 2022. Peridynamic Damage Model Based on Absolute Bond Elongation. International Conference on Computational Science, 637-650.
[36] Zhang, S.Y., Nie, Y.F., Li, Y.Q., 2022. The RBF-PU Method for Solving 2D Nonlocal Diffusion and Peridynamic Equations. Appl. Math. Mech. 43(6), 608-618.
[37] Zhao, L., Liu, J.R., Wang, R. et al., 2017. Distribution Characteristics and Genesis Analysis of Ground Fissures in Songzhuang, Beijing. Shanghai Land Resour. 38(2), 35-38.
[38] Zhao, L., Luo, Y., Li, Y.M. et al., 2019. Morphological Characteristics and Influencing Factors of Ground Fissure Disaster Bodies in the Beijing Plain Area. J. Hydrogeol. Eng. Geol. 46(6), 156-164.
[39] Zuo, P.F., Liu, C., Guo, Q.Z., Feng, X., 2023. Numerical Simulation and Dispersion Characteristics Analysis of Crack Model Wavefield Based on Peridynamic Theory. J. Jilin Univ. 53(04), 1250-1261.

Hebei Cangzhou Groundwater and Land Subsidence National Observation and Research Station, Cangzhou 061000, China,

Key Laboratory of Mechanism, Prevention and Mitigation of land Subsidence, MOE, Capital Normal University, Beijing 100048, China,

Beijing Laboratory of Water Resources Security, Capital Normal University, Beijing 100048, China,
E-mail: wangche1835@126.com, wlfzzzzzz@163.com, 4039@cnu.edu.cn and 5099@cnu.edu.cn

China Institute of Geo-Environment Monitoring, Beijing 100081, China
E-mail: zangxisheng@mail.cgs.gov.cn and pengfei7971@shou.com